

Submitted to *Earth, Planets, and Space*

Seismicity prior to the 2016 Kumamoto earthquakes

Author #1: K. Z. Nanjo, Global Center for Asian and Regional Research, University of Shizuoka, 3-6-1, Takajo, Aoi, Shizuoka 420-0839, Japan, Tel: +81-54-245-5600, Fax: +81-54-245-5603, E-mail: nanjo@u-shizuoka-ken.ac.jp

Author #2: J. Izutsu, International Digital Earth Applied Science Research Center, Chubu Institute for Advanced Studies, Chubu University, 1200 Matsumoto-cho, Kasugai, Aichi 487-8501, Japan, Tel: +81-568-51-1111, Fax: +81-568-51-1642, E-mail: izutsu@isc.chubu.ac.jp

Author #3: Y. Orihara, Department of Physics, Tokyo Gakugei University, 4-1-1, Nukuikita, Koganei, Tokyo 184-8501, Japan, Tel +81-42-329-7484, Fax: +81-42-329-7484, E-mail: orihara@u-gakugei.ac.jp

Author #4: N. Furuse, Institute of Oceanic Research & Development, Tokai University, 3-20-1, Orido, Shimizu, Shizuoka 424-0902, Japan, Tel: +81-54-337-0946, Fax: +81-54-336-0920, E-mail: furuse@sems-tokaiuniv.jp

Author #5: S. Togo, Department of Physics, Tokyo Gakugei University, 4-1-1, Nukuikita, Koganei, Tokyo 184-8501, Japan, Tel +81-42-329-7484, Fax: +81-42-329-7484, E-mail: f117126w@st.u-gakugei.ac.jp

Author #6: H. Nitta, Department of Physics, Tokyo Gakugei University, 4-1-1, Nukuikita, Koganei,

Tokyo 184-8501, Japan, Tel +81-42-329-7484, Fax: +81-42-329-7484, E-mail:
a120349w@st.u-gakugei.ac.jp

Author #7: T. Okada, Department of Physics, Tokyo Gakugei University, 4-1-1, Nukuikita, Koganei, Tokyo 184-8501, Japan, Tel +81-42-329-7484, Fax: +81-42-329-7484, E-mail:
b142312x@st.u-gakugei.ac.jp

Author #8: R. Tanaka, Department of Physics, Tokyo Gakugei University, 4-1-1, Nukuikita, Koganei, Tokyo 184-8501, Japan, Tel +81-42-329-7484, Fax: +81-42-329-7484, E-mail:
f117124x@st.u-gakugei.ac.jp

Author #9: M. Kamogawa, Department of Physics, Tokyo Gakugei University, 4-1-1, Nukuikita, Koganei, Tokyo 184-8501, Japan, Tel +81-42-329-7484, Fax: +81-42-329-7484, E-mail:
kamogawa@u-gakugei.ac.jp

Author #10: T. Nagao, Institute of Oceanic Research & Development, Tokai University, 3-20-1, Orido, Shimizu, Shizuoka 424-0902, Japan, Tel: +81-54-337-0946, Fax: +81-54-336-0920, E-mail:
nagao@scc.u-tokai.ac.jp

Corresponding author: T. Nagao

Abstract

We report precursory seismic patterns prior to the 2016 Kumamoto earthquakes, as measured by four different methods based on changes in seismicity that can be used for earthquake forecasting: the *b*-value method, two kinds of seismic quiescence evaluation methods, and an analysis of seismicity density in space and time. The spatial extent of precursory patterns differs from one method to the other and ranges from local scales (typically asperity size) to regional scales (e.g., 2° ×

3° around the source zone). The earthquakes were preceded by periods of pronounced anomalies, which lasted in yearly scales (1~1.5 years), or longer (>3 years). We demonstrate that a combination of multiple methods detected different signals prior to the Kumamoto earthquakes with greater reliability than if measured by a single method. This indicates great potential to reduce possible future sites of earthquakes relative to long-term seismic hazard assessment.

Keywords: Crustal deformation; Earthquake, Tsunami; Physical property of rocks; Time-series analysis; Probabilistic forecasting; Computational seismology; Statistical seismology; 2016 Kumamoto earthquakes; Critical phenomenon; Foreshocks

Introduction

The 2016 Kumamoto earthquakes, including a magnitude $M7.3$ mainshock that struck on April 16, 2016, as well as active foreshocks and aftershocks, fulfilled a section of the Futagawa-Hinagu fault zones. The zones are encompassed by the Beppu-Shimabara graben, a geological formation that runs across the middle of Kyushu, from Beppu Bay in the east to the Shimabara Peninsula in the west. This is understood as being the result of crustal deformation caused by the rifting and spreading of the Okinawa Trough, which is viewed as a continuation of the Beppu-Shimabara graben (Tada, 1985). The November 14, 2015 $M7.1$ earthquake occurred off Satsuma Peninsula in the Okinawa Trough. This event and the Kumamoto earthquakes are considered to be the onset that occurred under the same tectonics (Ishibashi, 2016).

A wide variety of approaches have been applied to earthquake prediction and forecasting. Most proposed prediction and forecasting methods rely on the concept of a diagnostic precursor; i.e., some kind of signal observable before earthquakes that indicates with high probability the location,

time, and magnitude of an impending event. Precursor methods include changes in strain rates, seismic wave speeds, and electrical conductivity; variations of radon concentrations in groundwater, soil, and air; fluctuations in groundwater levels; electromagnetic variations near and above the Earth's surface; and seismicity patterns. Despite this, the search for diagnostic precursors has not yet produced a successful short-term prediction scheme (e.g., Keilis-Borok, 2002; Scholz, 2002; Kanamori, 2003; International Commission on Earthquake Forecasting for Civil Protection, 2011).

Despite such a notable lack of success, there has been a resurgence of research on earthquake predictability motivated by better monitoring networks and data on past events, new knowledge of the physics of earthquake ruptures, and a more comprehensive understanding of stress evolution and transfer. The California and international working groups, RELM (Field 2007) and CSEP (Jordan, 2006), have been supporting research on earthquake predictability, conducting scientific experiments under rigorous, controlled conditions and evaluating them using accepted criteria specified in advance. These groups point to future directions of model development of earthquake prediction and forecasting as well as its testing. However, making full use of currently available resources for and a new knowledge and understanding of seismology, there needs predictability research that is not directly associated with the RELM and CSEP, but rather that addresses more general questions about the improvement of different hypotheses on earthquake generation and different concepts related to diagnostic precursor.

Different methods exist to measure, map, and evaluate possible episodes before mainshocks. Examples include the *b*-value method (e.g., Schorlemmer and Wiemer, 2005; Nanjo et al., 2012), RTL/RTM-algorithms (e.g., Sobolev and Tyupkin, 1997; Nagao et al., 2011), the Z-value method (e.g., Wiemer and Wyss, 1994; Wyss et al., 2004; Katsumata, 2015), and seismicity density

analysis (Lippiello et al., 2012). To our knowledge, there is no standardized approach that encourages researchers to rely exclusively on a single method. Instead, multiple methods must be used to find evidence of precursory episodes. One disadvantage is that the results obtained by different methods may not be easily compared, although one may gain more confidence in impending earthquakes when using different methods. Also, additional insight may be gained because of intrinsic differences in the statistical characterization of seismic patterns. Early attempts were made by Wyss et al. (2004) who used the RTL-algorithm and Z-value methods and by Enescu and Ito (2001) who used the *b* value and Z-value methods, and a fractal dimension approach.

This paper reports the first results of recognizing seismic patterns as possible precursory episodes to the 2016 Kumamoto earthquakes using existing four different methods: the *b* value method, two kinds of seismic quiescence evaluation methods (RTM-algorithm and Z-value), and seismicity density analysis. These methods are based on different assumptions, selection of sampling volumes, algorithms, and definitions of anomalies, thus they are representative of a wide variety of methods that can be used to detect precursory anomalies. Before presenting further details of our study, we present a brief overview of the methods that were used.

Methods

The b value method: The *b* value is the slope of the Gutenberg-Richter (GR) frequency-magnitude distribution of earthquakes (Gutenberg and Richter, 1944), $\log_{10}N = a - bM$, where N is the cumulative number of earthquakes of M or greater, a is the earthquake productivity of a volume, and b is used to describe the relative occurrence of large and small events (i.e., a high *b* value indicates a larger proportion of small earthquakes, and vice versa). Spatial and temporal

changes in b are known to reflect a structural heterogeneous structure (e.g., Mogi, 1962) such as strong coupling along subduction zones and a magma chamber (e.g., Tormann et al., 2015). In the laboratory and the Earth's crust, the b value is also known to be inversely dependent on differential stresses (Scholz, 1968, 2015). In this context, measurements of spatial temporal changes in b could act as a stress meter to help image asperities, the highly stressed patches in faults where future ruptures are likely to occur (e.g., Schorlemmer and Wiemer, 2005; Nanjo et al., 2012).

The RTM-algorithm: This is a type of weighted method that assesses the time, space and the size of earthquakes, and is a modified RTL algorithm (e.g., Sobolev and Tyupkin, 1997, 1999, Huang and Nagao, 2002, Huang, 2004, 2006, Sobolev, 2011). The RTM-algorithm measures the level of seismic activity in moving windows by counting the number of earthquakes that are weighted by their size and inversely weighted by their distances in time and space from the point of observation. A detailed description is provided by Nagao et al. (2011). A decrease of the *RTM* value implies a decrease in seismicity compared to the background rate around the investigated location (a seismic quiescence). A recovery stage from quiescence to the background level can be broadly considered as foreshock activation. The RTM-method evaluates both seismic quiescence and the following stage of activation. In addition, the location of maximum expression of an anomaly can be found by performing RTM-calculations with the centers of the sampling circles at the nodes of a grid.

The Z-value method: The Z-mapping approach measures the difference in seismicity rate, within moving time windows, to the background rate by a standard deviation, Z (Wiemer and Wyss, 1994; Wyss et al., 2004; Katsumata, 2015). The purpose is to detect possible periods of anomalously low seismicity just before the mainshock near its epicenter, and to evaluate the statistical

significance of such quiescence compared with all other rate-related decreases that may have occurred at random times and locations. The standard deviation Z is defined as $Z = (R_1 - R_2)/(S_1/n_1 + S_2/n_2)^{1/2}$, where R_1 and R_2 are the mean rates, S_1 and S_2 are the variances, and n_1 and n_2 are the number of events in the first and second periods to be compared. The larger the Z -value, the more significant the observed difference.

Seismicity density analysis: An increase in the number of smaller magnitude events before large earthquakes is often observed. The linear density probability of earthquakes occurring before and after events defined as mainshocks, $\rho(\Delta r)$, as a function of the distance from the mainshock hypocenter, Δr , displays a symmetrical behavior, indicating that the size of the area fractured during the mainshock is encoded in the spatial organization before the mainshock (Lippiello et al., 2012). The analysis based on Lippiello et al. (2012), hereinafter referred to as the seismicity density analysis, can be implemented to forecast the size of the mainshock. The objective of this paper is to detect such symmetric behavior for the Kumamoto earthquakes and to evaluate the possible size of the preparatory areas to the earthquakes.

Data

Our dataset is the earthquake catalog maintained by the Japan Meteorological Agency (JMA). We mainly used earthquakes since 2000, the start of modernization of the seismic networks feeding data to JMA (Obara et al., 2005). Since aftershocks add noise to both the Z -value method and the RTM-algorithm, we used a declustered catalog as a basic input for these methods. We eliminated aftershocks using the JMA standard declustering program (For details, see Appendix 1 and Fig. A1 in Additional file 1), which is classified as a link algorithm (Frolich and Davis, 1990).

A reliable estimate of completeness magnitude M_c , above which all earthquakes are considered to be detected by a seismic network, is vital for seismicity-related studies. We paid attention to catalog completeness, and performed a completeness check as a pre-processing step of individual analyses while referring to a comprehensive analysis of M_c in Japan (Nanjo et al., 2010).

Results

The b value method

A map view (Fig. 1a) of b values based on seismicity over a period from 2000 to April 14, 2016 21:25 (immediately before the Kumamoto earthquakes) reveals a zone of low b values near the eventual epicenters of the mainshock and two $M6.5$ -class foreshocks. The characteristic dimension of unusually low b values in an approximately $0.3^\circ \times 0.3^\circ$ area in Fig. 1a is ≈ 30 km. The $M5$ earthquake on June 8, 2000 occurred near the mainshock hypocenter so that we excluded seismicity related to this event and created maps of b values (Fig. A2 in Additional file 1). These maps show that a zone of low b values is insensitive to this exclusion, indicating that the 2000 $M5$ earthquake is not the main cause of the low spatially-mapped b values in Fig. 1. Comparison with the mainshock rupture zone (National Research Institute for Earth Science and Disaster Resilience, 2016) shows the influence of structural heterogeneity on spatial distribution in b values in such a way that rupture propagation of the mainshock terminated an area near Mt. Aso with $b \sim 1$, higher than b values within the rupture zone ($b = 0.6\sim0.8$). The high-temperature area around the magma chamber of Mt. Aso may have contributed to termination of the rupture (Yagi et al., 2016) and high b values (e.g., Roberts et al., 2015). We compared the map in Fig. 1a with the sequence of foreshocks, mainshock, and aftershocks with $M5$ or greater. Areas of low b values contained 84% of the sequence (Fig. A3

in Additional file 1). Two of the three aftershock regions, which lay further to the northeast, were observed around the high b value zones near Mt. Aso and Mt. Yufu, as observed in previous studies about b value characterization of volcanic systems (e.g., Roberts et al., 2015).

For earthquakes in the cylindrical volume with a radius $R = 10$ km, centered at the epicenter of the mainshock (Fig. 1c), there is time independence in b values after the fluctuation in b due to aftershocks of the 2000 $M5$ earthquake within this volume (See also Fig. A4 in Additional file 1). The precursory duration of the b -value is unknown, because the time variation in b shows no clear change-point during the analyzed period. A similar time-series analysis was performed for seismicity in the Futagawa, Hinagu, Aso-Kuju, and Beppu fault zones (See Figs. A5-A9 in Additional file 1). The b values show no systematic increase or decrease for all fault zones. A summary of the results is provided in Table 1.

RTM-algorithm

As described in the Data section, we first eliminated aftershocks. Next, we conducted a completeness analysis of the JMA catalog for the study region (Fig. 2) and obtained typically $M_c = 2$ so that we primarily set a lower threshold at $M_{\min} = 2$. Then, through an extensive parameter survey, we found anomalous seismic quiescence patterns as explained next.

A temporal variation of *RTM* at an almost equidistant point from the 2015 Off Satsuma Peninsula earthquake and the 2016 Kumamoto mainshock showed a significant decrease prior to the occurrence of both (Fig. 2a, see also Table A1 in Additional file 1). A deviation from the background started at 2014.7 years and the strongest deviation in October 2015 (2015.8 years) was about -20. During the critical period, the R , T , and M functions attained values of about -2.5~-3.0. A

recovery stage from the quiescence to the background level occurred in the last stage. This property is similar to that documented by other studies that used the RTL/RTM-algorithm (e.g., Sobolev and Tyupkin, 1997, 1999, Huang and Nagao, 2002, Huang, 2004, 2006; Nagao et al., 2011, Sobolev, 2011). Since the RTM algorithm is statistical and nonlinear, we were unable to identify which of earthquakes contributed to the recovery stage; this topic is beyond the scope of our work in this paper.

A map view of *RTM* values on October 1, 2015 reveals a highly significant change between the two mainshocks (Fig. 2b), in which the parameter set was the same as that for Fig. 2a. The characteristic dimension of seismic quiescence in an approximately $2^\circ \times 3^\circ$ area is 200~300 km. We created a map of *RTM* values using the same parameter set as that for Fig. 2b except that a higher threshold ($M_{\min} = 2.4$) was applied. The position of the anomalous zone is not very sensitive (See Panel E of Fig. A10 in Additional file 1). We also used three different sets of parameters with $M_{\min} = 2$ and created *RTM* maps to support a more robust anomalous pattern (See Panels A-C of Fig. A10 and Table A1 in Additional file 1).

To strengthen the related conclusion, it would be better to conduct a reliability analysis of the revealed anomalies in detail, e.g., following the approach taken by Huang (2006). However, the main purpose of this paper was to provide the first results on how to recognize possible precursory episodes to the 2016 Kumamoto earthquakes, as described in the Introduction. Thus, we presented essential parts of the reliability analysis such as completeness check, quality test of a declustered catalog, and some levels of a parameter survey. For a full justification of the present conclusion, further detailed investigations involving the robustness of the temporal and spatial pattern should be conducted. Thus, this paper prepares the groundwork for a future study in which

we test whether or not the anomaly reported in this paper is artificial, whether or not it correlates with an investigated event, and whether or not it is a random anomaly (Huang, 2006).

Our results do not indicate that the observed seismic quiescence precedes either of the mainshocks. The 2015 Off Satsuma Peninsula earthquake and the 2016 Kumamoto earthquakes are considered to be the onset that occurred at a section along the tectonic line from the Okinawa Trough through the Beppu-Shimabara graben (Ishibashi, 2016; Tada, 1985). Our results, combined with these tectonics, indicate that a series of earthquakes along the tectonic line was preceded by seismic quiescence. These results are summarized in Table 1.

The Z-value method

Similar to the RTM-algorithm, the processing steps were performed to ensure data quality. An extensive parameter survey was then conducted to choose the most suitable parameter set. The cumulative number of earthquakes with $M_{min} = 2.4$ as a function of time for a circle with sampling radius $R = 100$ km, centered at a point about 60 km away to the northeast from the epicenter of the 2015 Off Satsuma Peninsula mainshock, showed an anomaly of a few earthquakes during about 1 year before this mainshock (Fig. 3) and about 1.5 years before the Kumamoto mainshock. With a look-ahead time window $T_w = 1$ year, sampling radius $R = 100$ km, and $M_{min} = 2.4$, comparison of the seismicity rate during the last year before the Off Satsuma Peninsula mainshock with the background seismicity rate resulted in $Z = 2.9$. This representative result shows a typical precursory quiescence pattern to a large earthquake: fluctuation in Z at low levels followed by a rapid increase to high values. At other points, this typical pattern is degraded or unobservable, as shown in Fig. A11 in Additional file 1 (see a further parameter survey in Appendix 2 in

Additional file 1 that supports our results). Following the RTM-algorithm, we used a lower threshold at $M_{min} = 2.0$. Quiescence patterns were observed but this characteristic was degraded (Fig. A12 in Additional file 1). In summary, in the area with $R = 100$ km centered at a point about 60 km away to the northeast from the epicenter of the Off Satsuma Peninsula mainshock, the Z-value analysis detected a typical precursory quiescence, which lasted about 1 year (Table 1).

Seismicity density analysis

Before assuming the same approach as Lippiello et al. (2012) for Japan, a complete check of the JMA catalog since 1998 was performed as a pre-processing step. We decided to use inland earthquakes only and set a lower threshold at $M_{min} = 1$. The previous Z-value and RTM approaches were applied to data including both inland and offshore earthquakes (Figs. 2 and 3). M_c of the JMA catalog was generally lower in inland regions than offshore regions (Nanjo et al., 2010), which explains why $M_{min} = 1$ for this seismicity density analysis is different from $M_{min} = 2$ and 2.4 for the Z-value and RTM approaches.

As shown in the inset of Fig. 4 for mainshock magnitudes $4 \leq m < 5$, $\rho(\Delta r)$ before and after mainshocks was very similar in the whole spatial range for all magnitude ranges $m \in [3, 6]$, consistent with Lippiello et al. (2012). The decay of seismicity density with distance is well modeled by an inverse power-law $\rho(\Delta r) \sim \Delta r^{-\eta}$ at $\Delta r \gg 0$, where η is a constant of 1~2 (Richards-Dinger et al., 2010). We assumed a typical $\eta = 1.35$ (Felzer and Brodsky, 2006).

We next compared the size of spatial organization before and after mainshocks with the size of asperity (Fig. 4). As a representative of the former size, we detected the deviation point from a scaling relation $\rho(\Delta r) \sim \Delta r^{-\eta}$ (the inset in Fig. 4). This deviation point is defined as the

characteristic distance Δr_c , below which the scaling is no longer valid, due to large variance of seismicity density or low seismicity density at very short distances to the mainshock hypocenter, above a location uncertainty of ~ 100 m in the JMA catalog. We created a plot of Δr_c versus m for $m \in [3, 6]$ in Fig. 4. The latter size was based on the scaling between asperity area S_a and m (Somerville et al., 2015). Assuming a circular asperity $S_a = \pi l_a^2$ where l_a is the characteristic asperity radius, we included the l_a - m relation in Fig. 4. Data (grey points) show a positive correlation with large scatter, and the Δr_c - m correlation appears to be similar to the l_a - m relation. To support this idea, data from the Δr_c - m correlation needs to be increased in Fig. 4.

We next considered the Kumamoto case in Fig. 5. When using the same approach as Lippiello et al. (2012), the $M7.3$ shock and a preceding $M6.5$ shock were close to each other in space and time of the seismicity density analysis for $m=6\sim 7$. Therefore, we used seismicity subsequent to the $M7.3$ quake and seismicity prior to the $M6.5$ quake. Although Fig. 5 shows a scatter diagram, data (blue stars) of seismicity subsequent to the $M7.3$ quake are approximated by $\rho(\Delta r) \sim \Delta r^{-\eta}$ with $\eta = 1.35$ for distances $\Delta r \geq 8$ km ($\Delta r_c = 8$ km). As a reference, we applied the same procedure to seismicity subsequent to the $M6.5$ shock until $M7.3$ shock (red triangles) and $\rho(\Delta r) \sim \Delta r^{-\eta}$ with $\eta = 1.35$ being a reasonable approximation for $\Delta r \geq 4$ km ($\Delta r_c = 4$ km). Analysis of seismicity 3, 6, 12, and 18 years before the $M6.5$ shock (inset of Fig. 5) reveals that the inverse power-law is an approximation for data at distances around $\Delta r \geq 40$ km ($\Delta r_c = 40$ km), with density levels above the background implied from distant seismicity (grey shading). An inverse power-law with $\eta = 1.35$ was clearly observed for the 3 year period, although the exponent η showed a gradual increase over the past 18 years. Data of Δr_c for the Kumamoto case are included in Fig. 4. Although this figure still shows large scatter, it is reasonable that a positive correlation between Δr_c and m is comparable with

the l_a - m relation. The similar dependences on m indicate that the size of the spatial organization of seismicity is governed by the size of asperity (see Table 1 for a summary).

Discussion and conclusions

Although long-term probabilistic seismic-hazard assessment can be made in Japan (e.g., National Seismic Hazard Maps for Japan) and other seismically active regions, it is generally accepted that immediate local precursory phenomena are not seen ubiquitously. Prior to a volcanic eruption, increases in regional seismicity and surface movements are generally observed. In order to test the hypothesis of a local precursor for a fault system, the Parkfield Earthquake Predictability Experiment was initiated in 1985. The expected Parkfield earthquake occurred beneath the heavily instrumented region on September 28, 2004. No local precursory changes were observed (Lindh, 2005). In the absence of local precursory signals, the next question is whether broader anomalies develop and in particular whether there is anomalous seismicity.

Before attempting to identify precursory phenomena, a fundamental question is whether there are different forecast methods applicable to seismicity in a region of interest, in particular in Japan. This is the question that we addressed in this paper. We decided to use the b -value method, the RTM-algorithm, seismicity density analysis, and the Z -value method, and applied them to seismicity before the Kumamoto earthquakes. Our study is the first report on this theme after completing the modernization of seismic monitoring in Japan. Before this, an early attempt was made by Enescu and Ito (2001), who used the b -value method, the Z -value method, and fractal dimensions to discover premonitory quiescence followed by activation of seismicity about 2 years before the occurrence of the 1995 $M7.2$ Kobe earthquake. These authors conducted their study

before completing the modernization of seismic monitoring such that they used data with $M3.5$ or lower recorded by a local network maintained by Kyoto University, combined with data with $M > 3.5$ from the JMA catalog.

The combination of multiple methods may enhance the reliability of the revealed anomalies when compared to the reliability of a single method. We performed some comprehensive comparisons of the results from each method to support this claim. The properties of precursory episodes are summarized in Table 1. Estimates of the duration and spatial extent contain uncertainties, which depend on the approaches taken in the analysis. The durations were almost identical in both the RTM-algorithm and the Z-value method. In these methods, the resulting maximum expression of the anomalies did not coincide with the epicenters of the Kumamoto mainshock, nor of the Off Satsuma Peninsula mainshock. Furthermore, both methods did not identify the same locations for the anomalous maximum. Wyss et al. (2004) indicated a reason for the difference between methods in pinpointing the location of an anomaly. The weighting of results based on the size of the earthquakes, which is only done in the RTM method but not in the Z-value method, results in some differences in the estimated significance in most samples. Therefore, the maximum expression of the anomaly was not observed at exactly the same locations. The reason for the maximum expression of anomaly not pointing to the epicenters may be due to the fact that the onset of both earthquakes may have been at a segment along the tectonic line from the Okinawa Trough in the introduction. The large area of the anomaly may reflect the nature of the process leading up to the phenomenon in the regional tectonic condition. Nonetheless, the two methods based on different assumptions, different algorithms, and different definitions of anomaly, arrived at very similar results. This strongly suggests that the observed anomalies are real, and can be

determined with considerable reliability.

In contrast to these two methods, the *b*-value method and seismicity density analysis seem to have narrower spatial extents (Table 1). The close match found in spatial extent between the different approaches indicates that asperities (highly stressed patches) may indeed act as an indicator of the preparation process to an impending earthquake. A duration of 3 years or longer from the seismicity density analysis (Table 1) is longer than that revealed by both the RTM-algorithm and the *Z*-value method. The precursory duration from application of the *b*-value method to analyzed data for the past 16 years is unknown. The timing of the earthquake remains uncertain from low *b* values and spatial organization prior to the Kumamoto earthquakes. This is consistent with another observation of active faults in which the heterogeneous pattern of *b* values at Parkfield was, to a high degree, stationary for the past 35 years and the 2004 *M*6 earthquake eventually occurred at a zone of low *b* values (Schorlemmer and Wiemer, 2005). A decrease in *b* tracking stress buildup, as expected from a laboratory experiment (Scholz, 1968), may not be observable for the decade-scale observation of active faults in Japan and California, because it is too short to observe such a decrease in *b*. Instead, the stationary nature of *b* values, as observed in Fig. 1, is reasonable. The mechanism of stress buildup within the fault zones is uncertain, but one hypothesis is that a steady slip of the deeper continuation of faults that does not produce earthquakes, but still involves motions across the fault, forces the upper crust around the faults to bend and thus concentrate stress. This is still difficult to measure directly.

Overall, our findings indicate that the methods we adopted do not allow the Kumamoto earthquakes to be predicted exactly. However, the spatial extent of precursory patterns that were detected differed from one method to another and ranged from local scales (equivalent to an asperity

dimension), typically 30 km, to regional scales, typically 100~200 km. The Kumamoto earthquakes were preceded by periods of pronounced anomalies, which lasted yearly scales (typically 1~1.5 years) or longer (> 3 years). Given the widely different scales of anomalies in time and space, a combination of multiple methods was able to detect different signals prior to the Kumamoto earthquakes. If quantitative measurements involve multiple methods, the reliability of precursory anomalies to an impending earthquake is enhanced relative to the use of a single method. This strongly suggests a great potential to reduce possible future sites of earthquakes relative to long-term seismic hazard assessment.

This paper presents the first results obtained from a preliminary investigation into seismicity prior to the Kumamoto earthquakes. Comprehensive results based on in-depth analyses will be published elsewhere.

Competing interests

The authors declare no competing financial interests.

Authors' contributions

All the authors performed numerical simulations, analyzed data and prepare the figures: in particular, b value method (KZN, JI), RTM-algorithm (TN), Z-value method (KZN), seismicity density analysis (MO, ST, HN, TO, RT, MK), and application of declustering programs (KZN, NF, TN). KZN and TN helped to draft the manuscript. KZN wrote the final manuscript. All the authors read and approved the final manuscript.

Acknowledgements

The authors thank two anonymous referees for their useful comments. This study was partly supported by the Ministry of Education, Culture, Sports, Science and Technology (MEXT) of Japan, under its Earthquake and Volcano Hazards Observation and Research Program (KZN, JI, MO, MK, TN) and a Grant-in-Aid for Scientific Research (C), No. 26350483, 2014-2017 (MK), and the Collaboration Research Program of IDEAS, Chubu University IDEAS201614 (JI).

References

Enescu B, Ito K (2001) Some premonitory phenomena of the 1995 Hyogo-Ken Nanbu (Kobe) earthquake: seismicity, *b*-value and fractal dimension. *Tectonophysics* 338(3–4):297–314. doi:10.1016/S0040-1951(01)00085-3.

Felzer KR, Brodsky EE (2006) Decay of aftershock density with distance indicates triggering by dynamic stress. *Nature* 441:735–738. doi:10.1038/nature04799.

Field EH (2007) Overview of the working group for the development of regional earthquake likelihood models (RELM). *Seismol Res Lett* 78:7–16. doi:10.1785/gssrl.78.1.7.

Frohlich C, Davis SD (1990) Single-link cluster analysis as a method to evaluate spatial and temporal properties of earthquake catalogues. *Geophys J Int* 100(1):19–32. doi:10.1111/j.1365-246X.1990.tb04564.x.

Gutenberg B, Richter CF (1944) Frequency of earthquakes in California. *Bull Seismol Soc Am* 34(4):185–188.

Huang Q (2004) Seismicity pattern changes prior to large earthquakes - An approach of the RTL algorithm. *TAO* 15(3):469–491.

Huang Q (2006) Search for reliable precursors: A case study of the seismic quiescence of the 2000

western Tottori prefecture earthquake. J Geophys Res 111:B04301.

doi:10.1029/2005JB003982.

Huang Q, Nagao T (2002) Seismic quiescence before the 2000 $M=7.3$ Tottori earthquake. Geophys

Res Lett 29(12):19-1-19-4. doi:10.1029/2001GL013835.

International Commission on Earthquake Forecasting for Civil Protection (2011) Operational

earthquake forecasting. State of knowledge and guidelines for utilization. Ann Geophys 54(4).

doi: 10.4401/ag-5350.

Ishibashi K (2016) The 2016 Kumamoto earthquakes are not exceptional. Kagau (Science) 86(6):

532-540. In Japanese.

Jordan T (2006) Earthquake predictability, brick by brick. Seismol Res Lett 77:3–6.

Kanamori H (2003) Earthquake prediction: An overview, In: Lee WHK, Kanamori H, Jennings PC,

Kisslinger C (Eds) International handbook of earthquake & engineering seismology,

Academic Press, Amsterdam, pp. 1205–1216.

Katsumata K (2015) A long-term seismic quiescence before the 2004 Sumatra (Mw 9.1) earthquake.

Bull Seismol Soc Am 105(1):167-176. doi:10.1785/0120140116.

Keilis-Borok V (2002) Earthquake predictions: State-of-the-art and emerging possibilities. Ann Rev

Earth Planet Sci 30:1–33. doi:10.1146/annurev.earth.30.100301.083856.

Lindh AG (2005) Success and failure at Parkfield. Bull Seismol Soc Am 76(1):3-6.

doi:10.1785/gssrl.76.1.3.

Lippiello E, Marzocchi W, de Arcangelis L, Godano C (2012) Spatial organization of foreshocks as

a tool to forecast large earthquakes. Sci Rep 2:846. doi:10.1038/srep00846.

Mogi K (1962) Magnitude-frequency relation for elastic shocks accompanying fractures of various materials and some related problems in earthquakes. *Bull Earthq Res Inst* 40:831-853.

Nagao T, Takeuchi A, Nakamura K (2011) A new algorithm for the detection of seismic quiescence: introduction of the RTM algorithm, a modified RTL algorithm. *Earth Planet Space* 63:315–324. doi:10.5047/eps.2010.12.007.

Nanjo KZ, Hirata N, Obara K, Kasahara K (2012) Decade-scale decrease in *b* value prior to the *M*9-class 2011 Tohoku and 2004 Sumatra quakes. *Geophys Res Lett* 39:L20304. doi:10.1029/2012GL052997.

Nanjo KZ, Ishibe T, Tsuruoka H, Schorlemmer D, Ishigaki Y, Hirata N (2010) Analysis of the completeness magnitude and seismic network coverage of Japan. *Bull Seismol Soc Am* 100(6):3261-3268. doi:10.1785/0120100077.

National Research Institute for Earth Science and Disaster Resilience (2016) http://www.kyoshin.bosai.go.jp/kyoshin/topics/Kumamoto_20160416/inversion/. Access 20 Sept 2016.

Obara K, Kasahara K, Hori S, Okada Y (2005) A densely distributed high-sensitivity seismograph network in Japan: Hi-net by National Research Institute for Earth Science and Disaster Prevention. *Rev Sci Instrum* 76:021301. doi:10.1063/1.1854197.

Richards-Dinger K, Stein RS, Toda S (2010) Decay of aftershock density with distance does not indicate triggering by dynamic stress. *Nature* 467:583–586. doi:10.1038/nature09402.

Roberts NS, Bell AF, Main IG (2015) Are volcanic seismic *b*-values high, and if so when? *J Volcanol Geotherm Res* 308:127–141. doi:10.1016/j.jvolgeores.2015.10.021.

Scholz CH (1968) The frequency-magnitude relation of microfracturing in rock and its relation to

earthquakes. *Bull Seismol Soc Am* 58(1):399-415.

Scholz CH (2002) The mechanics of earthquakes & faulting, 2nd edn. Cambridge University Press, Cambridge.

Scholz CH (2015) On the stress dependence of the earthquake *b* value. *Geophys Res Lett* 42:1399-1402. doi: 10.1002/2014GL062863.

Schorlemmer D, Wiemer S (2005) Microseismicity data forecast rupture area. *Nature* 434:1086. doi:10.1038/4341086a.

Shi Y, Bolt BA (1982) The standard error of the magnitude-frequency *b*-value. *Bull Seismol Soc Am* 72:1677-1687.

Sobolev GA (2011) Seismicity dynamics and earthquake predictability. *Nat Hazards Earth Syst Sci* 11:445-458. doi:10.5194/nhess-11-445-2011.

Sobolev GA, Tyupkin YS (1997) Low-seismicity precursors of large earthquakes in Kamchatka. *Volcanol Seismol* 18:433–446.

Sobolev GA, Tyupkin YS (1999) Precursory phases, seismicity precursors, and earthquake prediction in Kamchatka. *Volcanol Seismol* 20:615-627.

Sommerville P, Skarlatoudis A, Thio HK (2015) Source scaling relations of subduction earthquakes for strong ground motion and tsunami prediction. <http://earthquake.usgs.gov/research/external/reports/G13AP00028.pdf>. Access Sept 20, 2016.

Tada T (1985) Spreading of the Okinawa Trough and its relation to the crustal deformation in the Kyushu (2). *Zisin* 38(1):1-12. In Japanese with English abstract.

Tormann T, Enescu B, Woessner J, Wiemer S (2015) Randomness of megathrust earthquakes implied by rapid stress recovery after the Japan earthquake. *Nature Geosci* 8:152–158.

doi:10.1038/ngeo2343.

Wiemer S, Wyss M (1994) Seismic quiescence before the Landers ($M=7.5$) and Big Bear ($M=6.5$) 1992 earthquakes. *Bull Seismol Soc Am* 84(3):900-916.

Woessner J, Wiemer S (2005) Assessing the quality of earthquake catalogues: Estimating the magnitude of completeness and its uncertainty. *Bull Seismol Soc Am* 95:684–698.

doi:10.1785/0120040007.

Wyss M, Sobolev G, Clippard JD (2004) Seismic quiescence precursors to two $M7$ earthquakes on Sakhalin Island, measured by two methods. *Earth Planet Space* 56(8):725–740.

doi:10.1186/BF03353081.

Yagi Y, Okuwaki R, Enescu B, Kasahara A, Miyakawa A, Otsubo M (2016) Rupture process of the 2016 Kumamoto earthquake in relation to the thermal structure around Aso volcano. *Earth Planet Space* 68:118. doi:10.1186/s40623-016-0492-3.

Table 1. Characteristic precursory phenomena

Method	Spatial extent	Duration
b -value method	Area of $0.3^\circ \times 0.3^\circ$ containing a part of the source zone of the Kumamoto mainshock	Unknown
RTM-algorithm	Area of $2^\circ \times 3^\circ$ between the Kumamoto and Off Satsuma Peninsula mainshocks	1.5 years for the Kumamoto mainshock (1 year for the Off Satsuma Peninsula mainshock)
Z-value method	Area with $R = 100$ km between the Kumamoto and Off Satsuma Peninsula mainshocks	1.5 years for the Kumamoto mainshock (1 year for the Off Satsuma Peninsula mainshock)
Seismicity density analysis	Area with $\Delta r = 8\sim40$ km containing a part of the source zone of the Kumamoto mainshock	3 years or longer for the Kumamoto mainshock

Figure legends

Fig. 1. **a** Map of b values obtained from events from January 1, 2000 to April 14, 2016 21:25 (immediately before the Kumamoto earthquakes). Overlapped on the map are the hypocenter (yellow star) and rupture zone (rectangle) of the $M7.3$ mainshock; $M6.5$ -class foreshocks (red stars); $M \geq 5$ foreshocks (squares); and $M \geq 5$ aftershocks (circles). Triangles: volcanoes; red line: faults. We calculated b values (Woessner and Wiemer, 2005) for events with depths 25 km or shallower falling in a cylindrical volume with radius $R = 5$ km, centered at each node on a $0.02^\circ \times 0.02^\circ$ grid (we did not use a fixed number of earthquakes) and plotted a b value at the corresponding node only if at least 50 events in the cylinder yielded a good fit to the GR law. **b** GR fitting is shown for points A, B, and C in **a**. **c** Plot of b values as a function of time, as obtained from seismicity in the cylindrical volume with $R = 10$ km, centered at the mainshock. We used a moving window approach, whereby the window covered 500 events. Uncertainty estimates are according to Shi and Bolt (1982). Grey squares and open circles show the b values obtained from foreshocks and aftershocks, respectively. Horizontal line: regional average $b = 0.93$; vertical line: moment of the mainshock.

Fig. 2. **a** Temporal variations of the RTM (black), R (blue), T (green), and M (red) at the point indicated by a cross in **b**. Red arrows show the moments of the 2015 Off Satsuma Peninsula earthquake and the 2016 Kumamoto mainshock; both epicenters are indicated by stars in **b**. **b** Areas of seismic quiescence before the two earthquakes (stars). The figure, generated by a grid with $0.1^\circ \times 0.1^\circ$ spacing, shows the most quiescent period on October 1, 2015, indicated by a black arrow in **a** (45 days before the 2015 Off Satsuma Peninsula earthquake). The cross is the point of time variation shown in **a**. Parameters used were $R_0 = 100$ km, $R_{\max} = 200$ km, $T_0 = 1$ year, $T_{\max} = 2$ years, and M_{\min}

= 2 (Table A1 in Additional file 1). For parameter definition, see Nagao et al. (2011).

Fig. 3. Cumulative number of earthquakes (blue, scale on left) with $M \geq 2.5$ as a function of time, up to the occurrence of the Off Satsuma Peninsula earthquake in 2015.8 (star). Curve in red shows the Z-values (scale on right), resulting from every position of the time window $T_w = 1$ year. The sample is from a circle with $R = 100$ km, centered at the black dot in the inset. Also included in the inset for reference are stars showing the 2015 Off Satsuma Peninsula and the 2016 Kumamoto mainshocks, and grey dots showing the centers of the collecting volumes with $R = 100$ km to create Fig. A11 in Additional file 1.

Fig. 4. A plot of the characteristic distance Δr_c as a function of mainshock magnitude m for seismicity prior (circles) and subsequent (diamonds) to mainshocks in Japan. The Kumamoto earthquakes (see also Fig. 5) are shown as a set of data of prior and subsequent seismicity as follows: brown line segment from $m6.5$ to 7.3 with a brown circle, indicating seismicity during a 3-year period prior to the $M6.5$ shock; blue line segment from $m6.5$ to 7.3 with a blue diamond, indicating seismicity subsequent to the $M7.3$ shock. As a reference, data for seismicity in the period subsequent to the $M6.5$ shock until the $M7.3$ shock is included (red diamond). Solid line shows the scaling of the characteristic asperity radius l_a with m , based on Somerville et al. (2015). Dashed lines indicate the one-standard-deviation limits. The inset shows a plot of $p(\Delta r)$ for foreshocks (circles) and aftershocks (diamonds) as a function of Δr from the mainshock with $m = 4\sim 5$. Data are fitted with $p(\Delta r) \sim \Delta r^{-\eta}$ with $\eta = 1.35$. The deviation point, below which an inverse power-law is no longer valid, is marked by Δr_c .

Fig. 5. Plot of $\rho(\Delta r)$ as a function of Δr for the Kumamoto earthquakes. Blue stars: seismicity subsequent to the $M7.3$ shock. As a reference, data on seismicity subsequent to the $M6.5$ shock until the $M7.3$ shock are marked by red upward-pointing triangles. Also included in this figure is an inverse power law with an exponent $\eta = 1.35$. The characteristic distance Δr_c , below which an inverse power-law is no longer valid, is marked for respective data. The inset shows a plot for seismicity prior to the $M6.5$ shock for different periods: 18 years (crosses), 12 years (grey downward-pointing triangles), 6 years (yellow diamonds), and 3 years (brown circles). Data for the 3 year period are fitted with an inverse power-law with $\eta = 1.35$. The deviation point, below which an inverse power-law is no longer valid, is marked by Δr_c . Grey shading indicates distances larger than 55 km, beyond which data are referred to as background density levels.

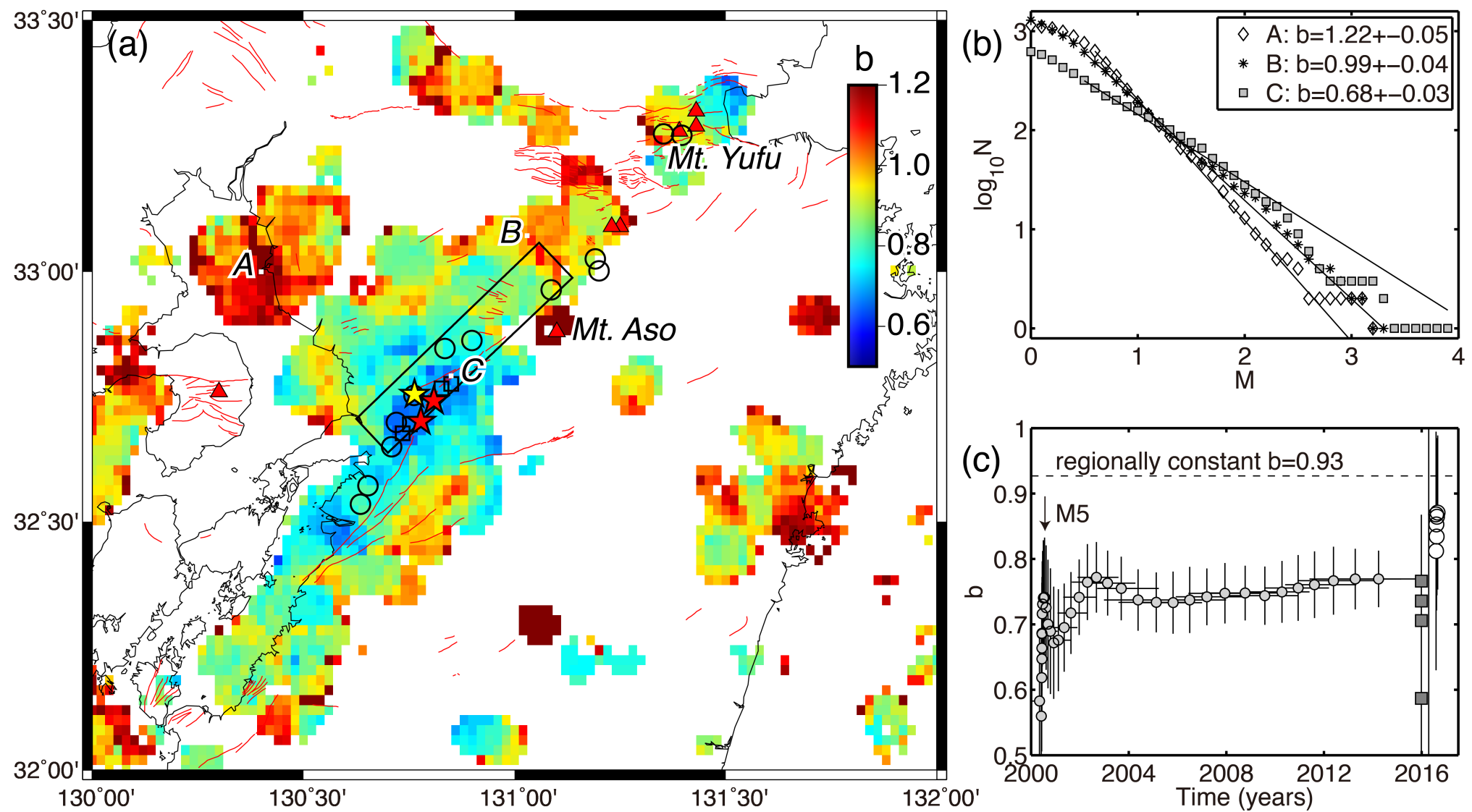


Fig. 1

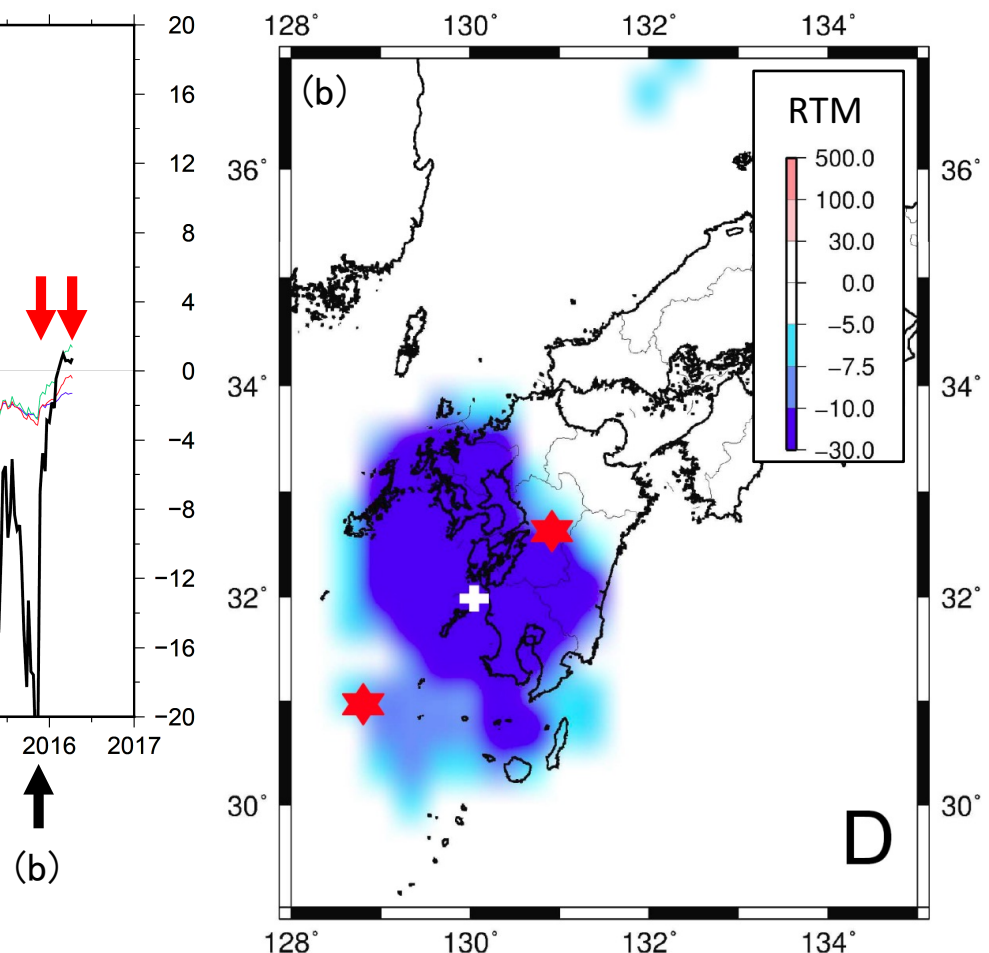
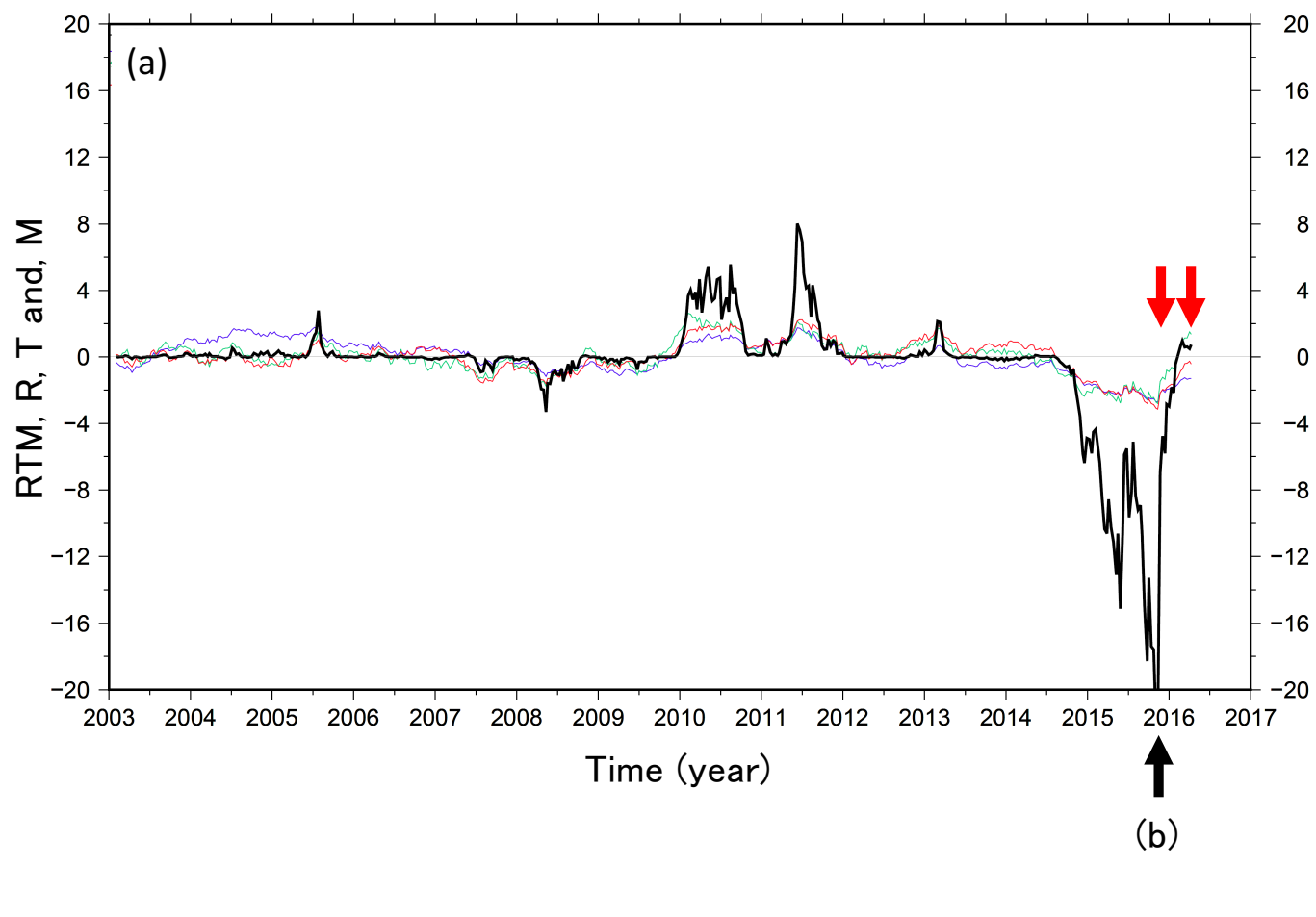


Fig. 2

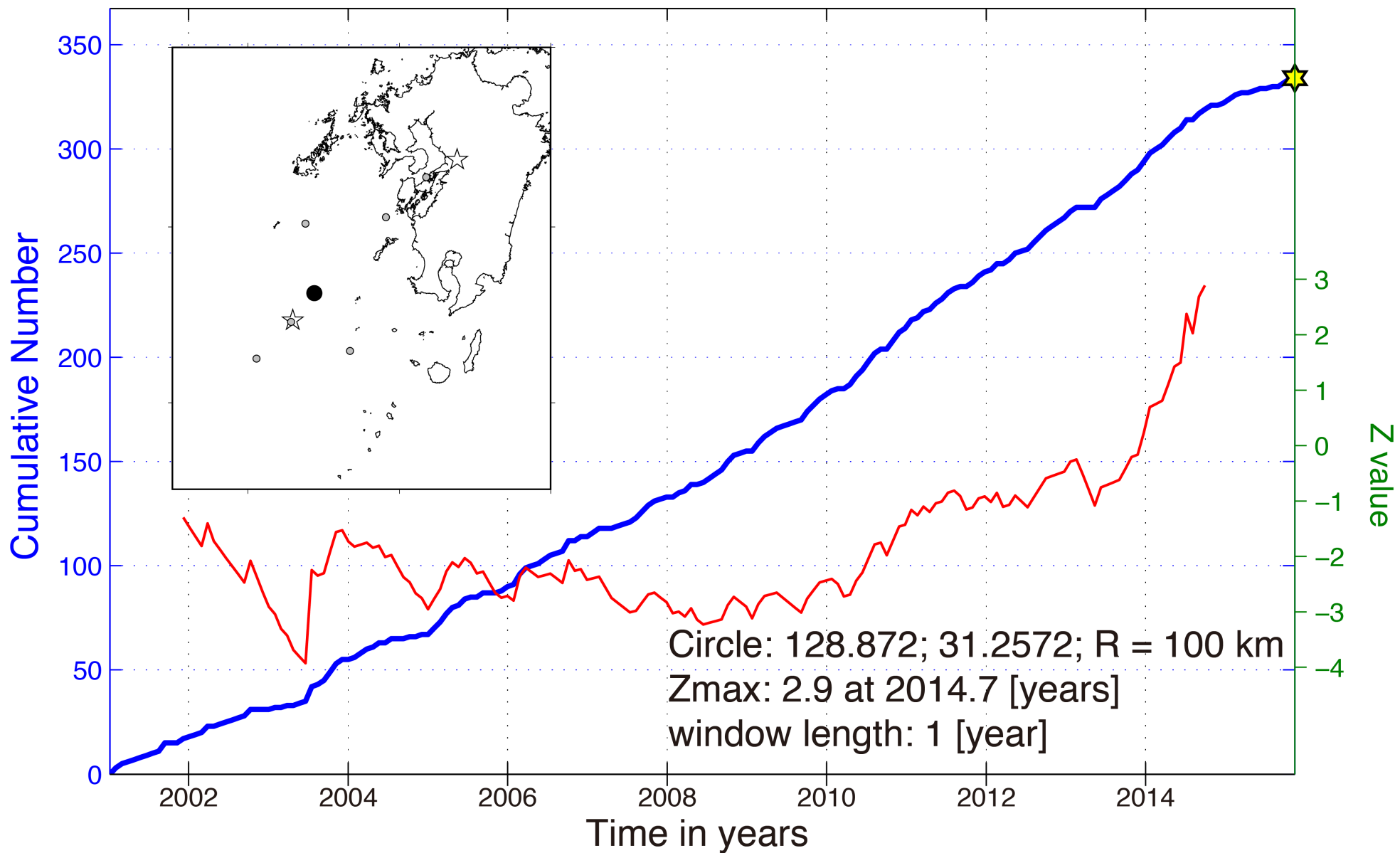


Fig. 3

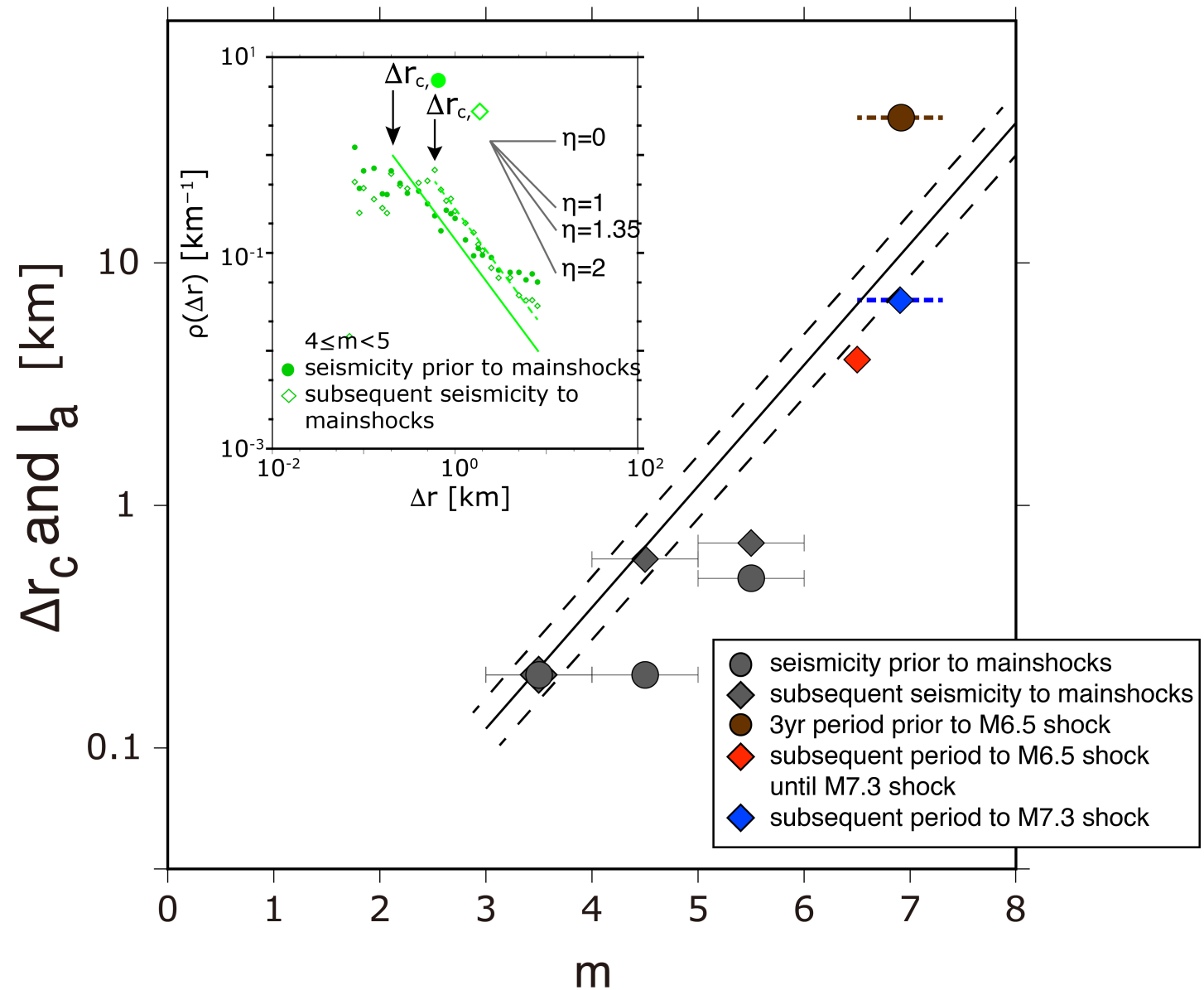


Fig. 4

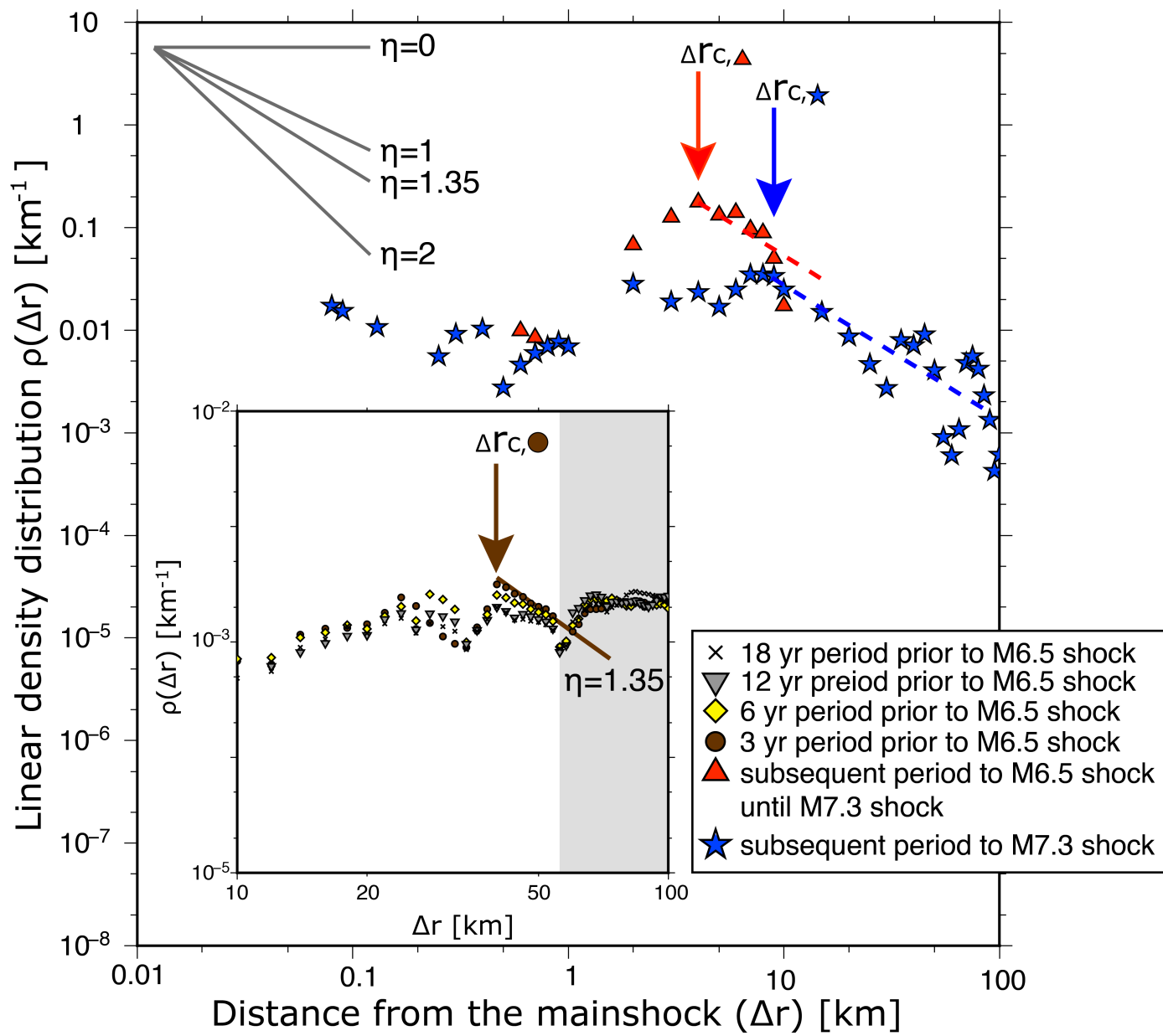


Fig. 5